Trefftz Finite Elements for Electromagnetics

Yuriy Olegovich Shlepnev, *Member, IEEE*

***Abstract*—It is shown that the method of minimum autonomous blocks (MAB) of Nikol'skii and Nikol'skaia can be reformulated as the Trefftz finite-element method. Solutions of Maxwell's equations in form of plane waves are used to represent fields inside a finite element. Their projections on a set of basis functions on the surface of the element are used to obtain a descriptor of the element in form of an admittance matrix. It is shown that a point-matching projection procedure gives the frequency-domain transmission-line-matrix formulation and Galerkin-type projection leads to the MAB formulation. Admittance matrix representation of the descriptors of the elements makes it possible to use a finite-element-type global matrix assembling procedure and a sparse matrix solver.**

***Index Terms*—Finite-element methods, transmission-line-matrix methods.**

I. Introduction

THE solution of boundary value problems for Maxwell's equations based on a division or decomposition of the problems into independently analyzed small volumes or blocks with following re-composition of scattering matrix descriptors of the blocks, called the method of minimum autonomous blocks (MAB), was first suggested by Nikol'skii and Nikol'skaia in the late 1970s [1], [2]. To find the descriptors of the minimal blocks, the authors proposed to solve a problem of diffraction of eigenmodes of some imaginary or virtual waveguides with cross sections corresponding to the faces of the block. Due to the diffraction nature of the problem formulation, scattering matrices were used as the descriptors of the blocks, which leads to a quite complex and nonstandard re-compositional procedure. In addition to the problem of finding eigenmodes of the virtual waveguides, which cannot be solved analytically for some interesting shapes (e.g., triangular), using Nikol'skii's procedure, the fields distribution inside the block has to be guessed, which makes it difficult to generalize on blocks, for instance, in the form of a triangular prism or tetrahedron.

As the story goes, Nikol'skii conceived the idea of MAB trying to understand the ideas of a network representation of three-dimensional (3-D) electromagnetic problems cultivated by Sestroretzkii in Russia and based on the work of Kron [3]. In his paper published in 1983, Sestroretzkii obtained time-domain, as well as frequency-domain scattering matrices of a so-called 3-D balanced node, which was later rediscovered in the West as the condensed node of the transmission-line-matrix (TLM) method by Johns [5] in the time domain and then by Jin and Vahldieck [6] in the frequency domain. Note that Sestroretzkii did not only deduce the scattering matrices using circuit-theory considerations, but also depicted the frequency- and time-domain equivalent circuits of the condensed node. Nikol'skii attempted to deduce the scattering matrix of the condensed node [2] using the MAB formulation and was able to do it only using Taylor's series expansions and dropping elements proportional to the cell size, which is not quite correct. That illustrates the difference between the basics of the MAB and TLM approaches, which are closely related, but in a different way, as will be shown in this paper.

Although the theory of MAB is correct and was fruitful in general, it was not popular in either Russia or in the West, probably due to ambiguities in the derivation procedure. Nikol'skii and Nikol'skaia obtained descriptors of the basic blocks in different coordinate systems and for different media, including anisotropic, and solved a very broad spectrum of problems, showing the immense potential of the approach. The TLM method found much broader support due to its relative simplicity. It was shown that the TLM method constitutes a finite-difference representation of Maxwell's equations [7], [8]. In those derivations, one has to know the resulting matrix at least roughly to be able to deduce it then or to prove that it approximates Maxwell's equations. There is also a derivation procedure based on the method of moments and cell boundary mapping and linear expansion functions [9] that is close to the approach suggested in this paper. The differential-geometry-based method of local approximation of Seredov [10] appears to be an alternative approach capable to provide TLM-like descriptors for volumes of different shape directly from Maxwell's equations.

In this paper, the method of MAB is reformulated as the Trefftz finite-element (TFE) method. The main idea of diffraction of eigenmodes of virtual waveguides on a minimal block is turned into an expansion of the electromagnetic fields inside the block into a set of solutions of Maxwell's equations in the form of plane waves. Boundary conditions on the surface of the block are then imposed using projections of the internal fields on a set of basis functions defined only on the surface of the element (two-dimensional (2-D) elements). This approach always gives the exact solution of Maxwell's equations inside the elements and approximates the boundary conditions, including the ones between the elements in a projection sense. The resulting element can be classified as the Trefftz-type finite element [11]. In addition to altering the conceptual basis of the MAB method, providing a systematic approach to build elements, this paper suggests to use admittance matrix descriptors of the elements instead of the scattering matrices. As a result, we obtain a transparent global matrix assembling procedure similar to the standard procedure of the finite-element method, which provides

Manuscript received September 14, 2000.

The author is with Innoveda Inc., Camarillo, CA 93010 USA (e-mail: yshlepnev@innoveda.com).

Publisher Item Identifier S 0018-9480(02)04054-1.

the possibility of using a readily available sparse matrix solver [11]. It also provides a simple and more natural procedure for boundary conditions superimposing and combining the method with the circuit theory.

Note that the authors of [1] and [2] presumably used the same procedure to "guess" the fields inside the blocks (he certainly needed to do it somehow), but this does not follow from their published works where the diffraction conception is promoted as the basis of the method.

To illustrate the TFE application, two different types of brick elements are constructed. A 12 plane-wave field expansion combined with point-matching projectors results in the admittance matrix description of a brick that can be reduced to the scattering matrix of the condensed TLM node in the frequency domain. The same 12 plane-wave field expansion, but with averaging or Galerkin's projectors on the surface of the brick, gives the admittance matrix, which can be converted to the scattering matrix of the brick MAB.

II. Problem Formulation

The problem formulation constitutes the scope of possible applications of TFEs. Consider a domain Ω composed of P nonoverlapping finite sub-domains Ω_p defined as

$$\Omega = \bigcup_{p=1}^{P} \Omega_p. \tag{1}$$

Each sub-domain Ω_p is filled with a homogeneous isotropic medium characterized by its properties as

$$\varepsilon(x, y, z) = \varepsilon_p \quad \mu(x, y, z) = \mu_p, \qquad (x, y, z) \in \Omega_p \tag{2}$$

where ε_p is the absolute permittivity of the sub-domain and μ_p is the absolute permeability of the sub-domain. Both are complex numbers in general and can be used to describe ideal and nonideal dielectrics, semiconductors, and nonideal metals. A sub-domain Ω_p has either common boundaries with some other sub-domains or is bounded by the electric or magnetic walls, surface impedance conditions, or by cross sections of semi-infinite waveguides where mode excitation and radiation conditions must be appropriately applied.

The electric ($\vec{E}^p$) and magnetic ($\vec{H}^p$) fields are related by Maxwell's equations inside a sub-domain p for a harmonic signal with the radian frequency ω

$$\left.\begin{aligned} &\nabla \times \vec{H}^p = i\omega\varepsilon_p \vec{E}^p \\ &\nabla \times \vec{E}^p = -i\omega\mu_p \vec{H}^p \\ &\nabla * \vec{E}^p = 0,\ \nabla * \vec{H}^p = 0 \end{aligned}\right\}, \qquad (x, y, z) \in \Omega^p \tag{3}$$

where $\times$ denotes vector products and $*$ denotes scalar products. We will denote a surface conduction current density on a common boundary of sub-domains l and m as $\vec{j}_{lm}$. Boundary conditions for the common boundary can be written as

$$\begin{aligned} &\overline{n} \times \left(\vec{H}^l(s_{lm}) - \vec{H}^m(s_{lm})\right) = \vec{j}_{lm} \\ &\overline{n} \times \left(\vec{E}^l(s_{lm}) - \vec{E}^m(s_{lm})\right) = 0, \qquad s_{lm} = \Omega_l \cap \Omega_m \end{aligned} \tag{4}$$

where $\overline{n}$ is the unit vector normal to the surface s_{lm}. To complete the problem formulation, we need to add boundary conditions on perfect or lossy metal and resistive film surfaces, magnetic-wall conditions, and the radiation and excitation conditions for waveguide cross sections. To model lumped-element connections, auxiliary port regions can be introduced on the boundaries between some sub-domains. The desired solution of the electromagnetic problem is an immitance matrix relating magnitudes of electric and magnetic fields of some eigenmodes on the waveguide cross-sectional boundaries and integral voltages and currents in all auxiliary port regions. To determine the propagation characteristics of the eigenmodes and corresponding matrices to transform the fields from the spatial to the eigenmode domain and to get a generalized descriptor of the problem, the method of "passage through the layer" [2], [12] or a simultaneous diagonalization method [13], [14] can be used.

III. Meshing Problem and Brick Element

Let us subdivide all regions of the problem using brick-shaped elements in a Cartesian coordinate system. All external and internal boundaries of the problem are mapped on surfaces of the brick elements that results in a stair–step approximation of the boundary conditions. The grid can be graded and adapted to the problem with some restrictions on connections between interfacing bricks. To obtain a high-quality mesh for a problem, one can use Cartesian mesh generation methods that are straightforward and simple in nature, very computationally effective, and well elaborated in the computational fluid dynamic [15].

One element of the grid is shown in Fig. 1, which from this point on is the main object under investigation. The element region is

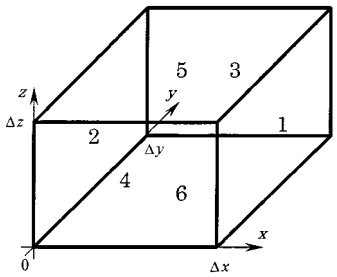

Fig. 1. Brick element.

$$\Omega_\Delta = \left\{(x, y, z),\ 0 \le x \le \Delta x,\ 0 \le y \le \Delta y,\ 0 \le z \le \Delta z\right\} \tag{5}$$

where Δx, Δy, and Δz are functions of the brick position in the space. The element is uniformly filled with a material (2)

defined by its permittivity ε and permeability μ. We drop the region indexes for simplicity.

Faces of the brick are numbered as is shown in Fig. 1 and are defined as

$$\begin{aligned}
F_1 &= \Big\{(\Delta x, y, z),\ 0 \le y \le \Delta y,\ 0 \le z \le \Delta z\Big\} \quad \overline{n}_1 = \overline{x}_0 \\
F_2 &= \Big\{(0, y, z),\ 0 \le y \le \Delta y,\ 0 \le z \le \Delta z\Big\} \quad \overline{n}_2 = -\overline{x}_0 \\
F_3 &= \Big\{(x, \Delta y, z),\ 0 \le x \le \Delta x,\ 0 \le z \le \Delta z\Big\} \quad \overline{n}_3 = \overline{y}_0 \\
F_4 &= \Big\{(x, 0, z),\ 0 \le x \le \Delta x,\ 0 \le z \le \Delta z\Big\} \quad \overline{n}_4 = -\overline{y}_0 \\
F_5 &= \Big\{(x, y, \Delta z),\ 0 \le x \le \Delta x,\ 0 \le y \le \Delta y\Big\} \quad \overline{n}_5 = \overline{z}_0 \\
F_6 &= \Big\{(x, y, 0),\ 0 \le x \le \Delta x,\ 0 \le y \le \Delta y\Big\} \quad \overline{n}_6 = -\overline{z}_0
\end{aligned} \tag{6}$$

where $\overline{x}_0$, $\overline{y}_0$, $\overline{z}_0$ are the unit vectors of the coordinate axes, and vector $\overline{n}_i$ defines the normal to the corresponding brick face F_i.

IV. Brick Interior Fields

Instead of defining the imaginary or virtual waveguides corresponding to the faces of the brick element and solving the corresponding diffraction problem as is suggested in the method of MAB [1], [2], we expand the field inside the element. For the brick containing isotropic filling with unknown conditions on the surface, the most general and natural expansion functions are solutions of Maxwell's equations in the form of plane waves. Let us choose three propagation directions along the coordinate axes. Each direction can be represented by the waves of two polarizations and each wave can travel forward and backward providing 12 total waves. This is the minimal number of waves for a general 3-D brick element. The field distribution inside the brick can be expressed as

$$\begin{aligned}
\begin{pmatrix}\vec{E}\\ \vec{H}\end{pmatrix} = {} & a_{x1}\cdot\begin{pmatrix}\overline{z}_0\\ -\overline{y}_0/Z_0\end{pmatrix}\cdot e^{-ikx} + b_{x1}\cdot\begin{pmatrix}\overline{z}_0\\ \overline{y}_0/Z_0\end{pmatrix}\cdot e^{ikx} \\
& + a_{x2}\cdot\begin{pmatrix}\overline{y}_0\\ \overline{z}_0/Z_0\end{pmatrix}\cdot e^{-ikx} + b_{x2}\cdot\begin{pmatrix}\overline{y}_0\\ -\overline{z}_0/Z_0\end{pmatrix}\cdot e^{ikx} \\
& + a_{y1}\cdot\begin{pmatrix}\overline{z}_0\\ \overline{x}_0/Z_0\end{pmatrix}\cdot e^{-iky} + b_{y1}\cdot\begin{pmatrix}\overline{z}_0\\ -\overline{x}_0/Z_0\end{pmatrix}\cdot e^{iky} \\
& + a_{y2}\cdot\begin{pmatrix}\overline{x}_0\\ -\overline{z}_0/Z_0\end{pmatrix}\cdot e^{-iky} + b_{y2}\cdot\begin{pmatrix}\overline{x}_0\\ \overline{z}_0/Z_0\end{pmatrix}\cdot e^{iky} \\
& + a_{z1}\cdot\begin{pmatrix}\overline{x}_0\\ \overline{y}_0/Z_0\end{pmatrix}\cdot e^{-ikz} + b_{z1}\cdot\begin{pmatrix}\overline{x}_0\\ -\overline{y}_0/Z_0\end{pmatrix}\cdot e^{ikz} \\
& + a_{z2}\cdot\begin{pmatrix}\overline{y}_0\\ -\overline{x}_0/Z_0\end{pmatrix}\cdot e^{-ikz} + b_{z2}\cdot\begin{pmatrix}\overline{y}_0\\ \overline{x}_0/Z_0\end{pmatrix}\cdot e^{ikz}
\end{aligned} \tag{7}$$

where $(x, y, z) \in \Omega_\Delta$, and a_{xl}, b_{xl}, a_{yl}, b_{yl}, a_{zl}, b_{zl}, $l = 1, 2$ are unknown coefficients of expansion, k is a propagation constant of a plane wave, and Z_0 is a characteristic impedance of the plane wave

$$k = \omega\sqrt{\varepsilon\mu} \quad Z_0 = \sqrt{\frac{\mu}{\varepsilon}}. \tag{8}$$

One can take any number of plane waves traveling in any directions to approximate some peculiarities of a problem, for instance, providing a corresponding number of projectors to obtain a defined system of equations for the unknown coefficients. Solutions in forms of cylindrical and spherical waves can be used to build elements for different coordinate systems. In general, any traveling-wave solution can be used to decompose the fields inside the element. The main principle is to use a minimal number of waves inside to obtain the best approximation quality. The conception can be generalized in the same way as Nikol'skii and Nikol'skaia generalized the conception of the MAB [2]. The generalized MAB's were called autonomous multimode blocks (AMBs). The idea was perfect, though the implementation contained a flaw. The AMBs obtained as the solutions of the diffraction problem of eigenmodes of the virtual rectangular waveguides corresponding to the brick faces had either zero electric fields or zero magnetic fields in all nodes of the brick, depending on the type of the waveguides used. It greatly limited the scope of the applications to the problems that could be decomposed into blocks with the nodes placed on the problem boundaries with corresponding zero boundary conditions.

V. Brick Surface Fields

With the plane-wave field expansion, defined in the previous section, it is natural and convenient to define basis functions for the faces F_1–F_6 (6) as a set of six pairs of constant vectors tangential to the corresponding faces and containing one unit component of electric and one unit component of the magnetic field. The face basis functions are denoted as

$$\overline{e}_{l(m)}, \overline{h}_{l(m)}, (x, y, z) \in F_l, \qquad l = 1, \ldots, 6; \quad m = 1, 2 \tag{9}$$

where l is the face number and m designates polarization. Vectors $\overline{e}_{l(m)}$ and $\overline{h}_{l(m)}$ are related to each other as

$$\overline{h}_{l(m)} = -(\overline{n}_l \times \overline{e}_{l(m)}) \tag{10}$$

where $\overline{n}_l$ is the normal to the corresponding face. Definition of the basis vectors in the form of (10) simplifies the boundary conditions (4) satisfaction in the global matrix assembling or re-composition procedure. The entire set of the electric-field expansion functions and their numeration is

$$\begin{aligned}
&1)\ \overline{e}_{1(1)} = \overline{z}_0 \quad 2)\ \overline{e}_{1(2)} = \overline{y}_0, && (x, y, z) \in F_1 \\
&3)\ \overline{e}_{2(1)} = \overline{z}_0 \quad 4)\ \overline{e}_{2(2)} = \overline{y}_0, && (x, y, z) \in F_2 \\
&5)\ \overline{e}_{3(1)} = \overline{z}_0 \quad 6)\ \overline{e}_{3(2)} = \overline{x}_0, && (x, y, z) \in F_3 \\
&7)\ \overline{e}_{4(1)} = \overline{z}_0 \quad 8)\ \overline{e}_{4(2)} = \overline{x}_0, && (x, y, z) \in F_4 \\
&9)\ \overline{e}_{5(1)} = \overline{x}_0 \quad 10)\ \overline{e}_{5(2)} = \overline{y}_0, && (x, y, z) \in F_5 \\
&11)\ \overline{e}_{6(1)} = \overline{x}_0 \quad 12)\ \overline{e}_{6(2)} = \overline{y}_0, && (x, y, z) \in F_6.
\end{aligned} \tag{11}$$

Fig. 2(a)–(c) illustrates the basis functions (11). Corresponding magnetic-field components are defined by (10). As an alternative, a complete set of vector basis functions can be obtained by solving Laplace's equations in the corresponding 2-D domain [2] or it can be chosen as a set of polynomial vector functions [16]. One can consider the faces as 2-D finite elements [11], which Nikol'skii called virtual waveguides. In

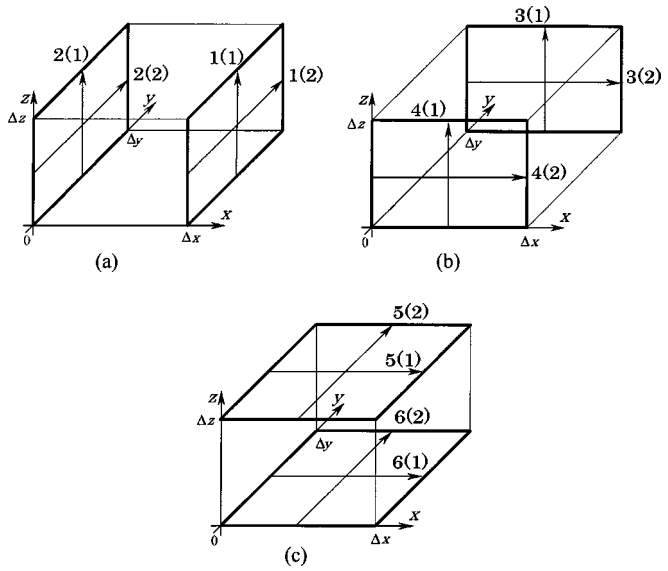

Fig. 2. Electric-field components of the basis functions. (a) For faces $F1$ and $F2$. (b) For faces $F3$ and $F4$. (c) For faces $F5$ and $F6$.

the method of MAB, Nikol'skii actually used solutions of the corresponding 2-D planar waveguide problems in the form of waves going inside and out of the brick to find its scattering matrix. A weak link in this approach is uncertainty in the boundary conditions and necessity to "guess" the field structure inside the element. One can still use the virtual waveguides conception in the TFE approach, but it must be clearly stated that they are only a set of functions to project the internal fields of the element to satisfy the boundary conditions between the elements. In addition, for triangular prisms or tetrahedrons, for example, it can be cumbersome to build the functions for the faces in the form of eigenwaves. The other vector functions can be considered in this case and combined with the appropriate number of plane waves inside the element.

Thus, the electric and magnetic field on the surface of the brick can be expanded into a set of vector basis functions (11) as follows:

$$\vec{E}_l = \sum_{m=1,\,2} v_{l(m)} \cdot \overline{e}_{l(m)}$$
$$\vec{H}_l = \sum_{m=1,\,2} i_{l(m)} \cdot \overline{h}_{l(m)}, \qquad (x, y, z) \in F_l; \quad l = 1, \ldots, 6. \tag{12}$$

To find unknown coefficients $v_{l(m)}$, $i_{l(m)}$, or rather their matrix dependency, we will use two projection operators. The first and simplest one is the point matching. In this case,

$$v_{l(m)} = \int_{F_l} \vec{E}(F_l) * \overline{e}_{l(m)} \cdot \delta_l \cdot \, ds$$
$$i_{l(m)} = \int_{F_l} \vec{H}(F_l) * \overline{h}_{l(m)} \cdot \delta_l \cdot ds, \qquad l = 1, \ldots, 6; \quad m = 1,\, 2 \tag{13}$$

where δ_l is the Dirac delta function that is equal to zero everywhere, except one point in the center of the face F_l, where it is equal to the unit. $\vec{E}(F_l)$ and $\vec{H}(F_l)$ are values of the electric and magnetic fields defined by (7) on the face of F_l. The point-matching procedure gives TFE that is referred to here as Trefftz finite elements of Sestroretzkii (TFES) because Sestroretzkii actually obtained a similar description of the element for a particular case of a cubic element [4] using different network considerations. A similar network-based deduction procedure of the condensed TLM node descriptor was later suggested by Johns [5] and used later in the frequency domain [8].

Another possibility of projecting the internal field of the brick on its surface is to test tangential to the surface fields with the expansion functions $\overline{e}_{l(m)}$ and $\overline{h}_{l(m)}$, which gives the Galerkin's projection procedure

$$v_{l(m)} = \frac{1}{N_l} \int_{F_l} \vec{E}(F_l) * \overline{e}_{l(m)} \, ds$$
$$i_{l(m)} = \frac{1}{N_l} \int_{F_l} \vec{H}(F_l) * \overline{h}_{l(m)} \, ds, \qquad l = 1, \ldots, 6; \quad m = 1,\, 2 \tag{14}$$

where

$$N_l = \int_{F_l} \overline{e}_{l(m)} * \overline{e}_{l(m)} \, ds = \int_{F_l} \overline{h}_{l(m)} * \overline{h}_{l(m)} \, ds \tag{15}$$

are norms of the expansion functions. Their values are

$$N_1 = N_2 = \Delta z \cdot \Delta y$$
$$N_3 = N_4 = \Delta z \cdot \Delta x$$
$$N_5 = N_6 = \Delta x \cdot \Delta y. \tag{16}$$

The projectors (14) can also be referred to as averaging projectors. They lead to a description of the element that can be converted into a scattering matrix descriptor of the method of MAB. Thus, the element obtained with the averaging projectors is called the Trefftz finite element of Nikol'skii (TFEN). Depending on a set of the basis functions defined on the surface and their orthonormality, another projectors can be considered.

With both projectors [i.e., (13) or (14)], the total number of unknown coefficients of the field expansion (12) on the brick surface is 24. This is twice as much as the number of the unknown expansion coefficients inside the brick (7). That means that by defining just 12 expansion coefficients on the surface of the brick, one can establish a relationship with the others and find the 12 remaining ones. It also means that any problem with uncertain boundary conditions on the brick surface can be described by a 12×12 descriptor matrix relating $v_{l(m)}$ and $i_{l(m)}$. In this paper, the descriptor matrix is built in an admittance form

$$Y \cdot \overline{v} = \overline{i} \quad Y \in C^{12 \times 12} \tag{17}$$

where $\overline{i}$ and $\overline{v}$ are vectors with 12 components defined by either (13) or (14) as follows:

$$\overline{i} = (\overline{i}_1, \overline{i}_2, \overline{i}_3, \overline{i}_4, \overline{i}_5, \overline{i}_6)^t$$
$$\overline{i}_l = \left(i_{l(1)}, i_{l(2)}\right)^t$$
$$\overline{v} = (\overline{v}_1, \overline{v}_2, \overline{v}_3, \overline{v}_4, \overline{v}_5, \overline{v}_6)^t$$
$$\overline{v}_l = \left(v_{l(1)}, v_{l(2)}\right)^t. \tag{18}$$

Superscript t in (18) denotes transposition. The admittance form (17) is convenient and natural for the re-composition of joining elements and for corresponding boundary condition superimposing. It leads to the standard matrix form formulation

accepted in the finite-element method [11]. To find the Y-matrix descriptor of the brick TFE, we assume that all surface expansion coefficients of the electric field are zero, except one $p(r)$, which is the unit

$$v_{l(m)} = \delta_{l(m),p(r)}, \qquad l = 1,\ldots,6; \quad m = 1, 2 \tag{19}$$

where $\delta_{l(m),p(r)}$ is the Kronecker delta. This numerical experiment gives the elements of the column $p(r)$ of the Y-matrix as projections of the corresponding magnetic fields

$$y_{l(m),p(r)} = i_{l(m)}, \qquad l = 1,\ldots,6; \quad m = 1, 2. \tag{20}$$

One can construct an immitance or mixed-type descriptor in general, mixing appropriately projections of the electric and magnetic fields in the left- and right-hand-side vectors of a system of equations similar to (17). It is a convenient to use such descriptors together with the admittance descriptors, for example, in places where it is necessary to impose the magnetic-wall boundary conditions.

VI. TFES

TFES is a brick TFE with descriptor obtained by the point-matching projections (13) of the brick internal fields (7) on the set of 24 2-D basis functions (11) defined on the surface of the brick. To find the elements of the admittance matrix of TFES, we will follow the numerical excitation procedure (19) that gives the equations for the matrix elements (20). Substitution of the expression for the electric field (7) inside the brick into the first equation of (13) and then into (19) provides 12 equations with 12 unknown coefficients a_{xl}, b_{xl}, a_{yl}, b_{yl}, a_{zl}, b_{zl}, $l = 1, 2$ per each out of 12 excitation states. Thus, one needs to solve 12 equations 12 times to find all elements of the Y-matrix (17). Fortunately, the problem is much simpler because of the symmetry of the equations (3) and geometrical symmetry of the brick. We need to solve the system only once to find the first column of the matrix, for example, and deduce the elements of the other columns applying substitutions and transformations similar to the ones suggested in [2]. Therefore, let us assume $v_{1(1)} = 1$, and the other projections of the electric field are zero. We obtain a system of 12 linear equations that can be divided into two independent systems. The first system is a system of eight homogeneous equations with a nondegenerate matrix. It has only the trivial solution

$$a_{x2} = b_{x2} = a_{y2} = b_{y2} = a_{z1} = b_{z1} = a_{z2} = b_{z2} = 0. \tag{21}$$

The second system of four equations is inhomogeneous and can be written as

$$\begin{bmatrix} 1/a^2 & a^2 & 1/b & b \\ 1 & 1 & 1/b & b \\ 1/a & a & 1/b^2 & b^2 \\ 1/a & a & 1 & 1 \end{bmatrix} \cdot \begin{bmatrix} a_{x1} \\ b_{x1} \\ a_{y1} \\ b_{y1} \end{bmatrix} = \begin{bmatrix} 1 \\ 0 \\ 0 \\ 0 \end{bmatrix} \tag{22}$$

where

$$a = e^{ik\Delta x/2} \quad b = e^{ik\Delta y/2}. \tag{23}$$

Solving (22) and substituting the resulting equations for the coefficients a_{x1}, b_{x1}, a_{y1}, b_{y1} into the equations for the magnetic fields inside the element (7) and then projecting them on the faces of the brick with the magnetic-field projectors (13) provides equations for the first column of the admittance matrix. By continuing the numerical excitation experiments for the other 11 projections of the electric field or, alternatively, using appropriate substitutions and transformations, it is possible to fill the other 11 columns of the admittance matrix (17). The final matrix is shown in (24) at the bottom of the following page, where

$$\begin{aligned} \alpha_1 &= f_\alpha(a, b) \\ \alpha_2 &= f_\alpha(a, c) \\ \alpha_3 &= f_\alpha(b, a) \\ \alpha_4 &= f_\alpha(b, c) \\ \alpha_5 &= f_\alpha(c, b) \\ \alpha_6 &= f_\alpha(c, a) \\ \beta_1 &= f_\beta(a, b) \\ \beta_2 &= f_\beta(a, c) \\ \beta_3 &= f_\beta(b, a) \\ \beta_4 &= f_\beta(b, c) \\ \beta_5 &= f_\beta(c, b) \\ \beta_6 &= f_\beta(c, a) \\ \gamma_1 &= f_\gamma(a, b) \\ \gamma_2 &= f_\gamma(a, c) \\ \gamma_3 &= f_\gamma(b, a) \\ \gamma_4 &= f_\gamma(b, c) \\ \gamma_5 &= f_\gamma(c, b) \\ \gamma_6 &= f_\gamma(c, a) \\ \delta_1 &= f_\delta(\Delta x) \\ \delta_2 &= f_\delta(\Delta y) \\ \delta_3 &= f_\delta(\Delta z). \end{aligned} \tag{25}$$

Functions $f_\alpha(p, q)$, $f_\beta(p, q)$, $f_\gamma(p, q)$, and $f_\delta(\Delta)$ in (25) are defined by expressions

$$\begin{aligned} f_\alpha(p, q) &= \frac{p^4(q^2+1) - 2p^3q - 2pq + q^2 + 1}{(p^2-1) f_{dn}(p, q)} \\ f_\beta(p, q) &= \frac{2p\left[p^2q - p(q^2+1) + q\right]}{(p^2-1) f_{dn}(p, q)} \\ f_\gamma(p, q) &= \frac{p(1-q^2)}{f_{dn}(p, q)} \\ f_{dn}(p, q) &= p^2(q^2+1) - 4pq + q^2 + 1 \\ f_\delta(\Delta) &= \frac{i}{2\sin(k\Delta/2)}. \end{aligned} \tag{26}$$

The parameters a and b are defined by (23) and c is defined as

$$c = e^{ik\Delta z/2}. \tag{27}$$

Let us now consider a particular case of the brick element descriptor (24) when all three dimensions of the brick are equal ($\Delta x = \Delta y = \Delta z = \Delta$). From (25) and (26) it follows that,

in this case, the Y-matrix is composed of only two different nonzero elements

$$\begin{aligned}
&\alpha_1 = \alpha_2 = \alpha_3 = \alpha_4 = \alpha_5 = \alpha_6 = \alpha \\
&\beta_1 = \beta_2 = \beta_3 = \beta_4 = \beta_5 = \beta_6 = 0 \\
&\gamma_1 = \gamma_2 = \gamma_3 = \gamma_4 = \gamma_5 = \gamma_6 = \delta_1 = \delta_2 = \delta_3 = \gamma \\
&\alpha = -i\cot(k\Delta/2) \\
&\gamma = \frac{i}{2\sin(k\Delta/2)}.
\end{aligned} \tag{28}$$

The inverted Y-matrix or impedance matrix of a cube looks similar to the initial matrix (24) with coefficients defined in (28). To obtain the impedance matrix, one needs to change the Y-matrix multiplier from $1/Z_0$ to Z_0 and change signs of all nondiagonal elements. In fact, the admittance and impedance matrices of the cube show the same relationship as the corresponding matrices of a segment of transmission line. Thus, this model of the cube can be considered a generalization of the transmission-line conception on 3-D structures (but it should not be confused with the multimode generalization). The equivalent circuit of the cube depicted by Sestroretzkii [4] illustrates the idea further. It can be shown that the inverted Y-matrix of the cube corresponds to the impedance matrix of the impedance analog of Maxwell's equations obtained in [17]. Elaborating further, we can deduce the frequency-domain TLM formulation. Let us introduce normalized projections of the electric and magnetic fields as

$$\tilde{v} = \frac{1}{\sqrt{|Z_0|}} \cdot \overline{v} \quad \tilde{i} = \sqrt{|Z_0|} \cdot \overline{i} \tag{29}$$

where $\overline{v}$ and $\overline{i}$ are defined by (18). We can now formally introduce incident and reflected waves defined as

$$\tilde{c}^+ = \frac{1}{2}\left(\tilde{v} + \tilde{i}\right) \quad \tilde{c}^- = \frac{1}{2}\left(\tilde{v} - \tilde{i}\right) \tag{30}$$

and a scattering matrix defined as

$$\tilde{c}^- = S \cdot \tilde{c}^+ \quad S \in C^{12\times 12}. \tag{31}$$

From (17) and (31)–(33), it follows that

$$S = (U - Z_0 Y) \cdot (U + Z_0 Y)^{-1} \tag{32}$$

where U is the unit matrix 12×12. Substitution of the Y-matrix (27) with the elements defined by (30) into (34) gives the scattering matrix of the cube, as shown in (33), at the bottom of the following page, where

$$\varphi = \frac{1}{2}\, e^{-ik\Delta/2} \quad \chi = 0. \tag{34}$$

The scattering matrix (33) corresponds to the one obtained by Sestroretzkii in [4], taking into account the difference between the numeration of the TFE basis functions and the balanced node ports. The TLM symmetrical condensed node derived by Johns in [5] does not contain the propagation delay factors (34) explicitly because of the time-domain formulation. The phase-shift exponents were added to the original TLM S-matrix later [18] to build the frequency-domain TLM condensed node. It can be shown that the S-matrix of a cubic TLM node without stubs in the frequency domain [18] corresponds to the S-matrix (33), obtained by the TFE method. Again, the difference in numeration of the TLM node ports must be taken into account.

VII. TFEN

TFEN is a brick TFE obtained with expansion of electric and magnetic fields inside the element into a set of 12 plane waves (7). The unknown coefficients of the expansion are found using an additional set of 24 expansion functions defined on the surface of the element (11) and the Galerkin's projections of internal fields on the faces of the brick (14). The admittance matrix (17) is chosen as a descriptor of the brick. Let us again perform the numerical experiments (19) to find the elements of the matrix using (20). The first experiment sets $v_{1(1)} = 1$ and 0 for the other 11 projections of the electric field. As with the point matching, we have a system of 12 linear equations with unknowns a_{xl}, b_{xl}, a_{yl}, b_{yl}, a_{zl}, b_{zl}, $l = 1, 2$, which can be

$$Y = \frac{1}{Z_0}\begin{bmatrix}
\alpha_1 & 0 & \beta_1 & 0 & \gamma_3 & 0 & \gamma_3 & 0 & \delta_3 & 0 & -\delta_3 & 0 \\
0 & \alpha_2 & 0 & \beta_2 & 0 & \delta_2 & 0 & -\delta_2 & 0 & \gamma_6 & 0 & \gamma_6 \\
\beta_1 & 0 & \alpha_1 & 0 & \gamma_3 & 0 & \gamma_3 & 0 & -\delta_3 & 0 & \delta_3 & 0 \\
0 & \beta_2 & 0 & \alpha_2 & 0 & -\delta_2 & 0 & \delta_2 & 0 & \gamma_6 & 0 & \gamma_6 \\
\gamma_1 & 0 & \gamma_1 & 0 & \alpha_3 & 0 & \beta_3 & 0 & 0 & \delta_3 & 0 & -\delta_3 \\
0 & \delta_1 & 0 & -\delta_1 & 0 & \alpha_4 & 0 & \beta_4 & \gamma_5 & 0 & \gamma_5 & 0 \\
\gamma_1 & 0 & \gamma_1 & 0 & \beta_3 & 0 & \alpha_3 & 0 & 0 & -\delta_3 & 0 & \delta_3 \\
0 & -\delta_1 & 0 & \delta_1 & 0 & \beta_4 & 0 & \alpha_4 & \gamma_5 & 0 & \gamma_5 & 0 \\
\delta_1 & 0 & -\delta_1 & 0 & 0 & \gamma_4 & 0 & \gamma_4 & \alpha_5 & 0 & \beta_5 & 0 \\
0 & \gamma_2 & 0 & \gamma_2 & \delta_2 & 0 & -\delta_2 & 0 & 0 & \alpha_6 & 0 & \beta_6 \\
-\delta_1 & 0 & \delta_1 & 0 & 0 & \gamma_4 & 0 & \gamma_4 & \beta_5 & 0 & \alpha_5 & 0 \\
0 & \gamma_2 & 0 & \gamma_2 & -\delta_2 & 0 & \delta_2 & 0 & 0 & \beta_6 & 0 & \alpha_6
\end{bmatrix} \tag{24}$$

divided into two independent systems. The first is a homogeneous system with a nondegenerate matrix that leads to a trivial solution (21). The second system of four equations is

$$\begin{bmatrix} \frac{1}{a} & a & \frac{1}{k_b}\left(1-\frac{1}{b}\right) & \frac{1}{k_b}(b-1) \\ 1 & 1 & \frac{1}{k_b}\left(1-\frac{1}{b}\right) & \frac{1}{k_b}(b-1) \\ \frac{1}{k_a}\left(1-\frac{1}{a}\right) & \frac{1}{k_a}(a-1) & \frac{1}{b} & b \\ \frac{1}{k_a}\left(1-\frac{1}{a}\right) & \frac{1}{k_a}(a-1) & 1 & 1 \end{bmatrix} \cdot \begin{bmatrix} a_{x1} \\ b_{x1} \\ a_{y1} \\ b_{y1} \end{bmatrix} = \begin{bmatrix} 1 \\ 0 \\ 0 \\ 0 \end{bmatrix} \quad (35)$$

where

$$k_a = ik\Delta x \quad k_b = ik\Delta y \quad a = e^{ik\Delta x} \quad b = e^{ik\Delta y}. \quad (36)$$

The solution of the system (35) and subsequent substitution of the resulting equations for the coefficients a_{x1}, b_{x1}, a_{y1}, and b_{y1} into (7) gives the expressions for the magnetic field inside the brick element. Projection of the magnetic field on the faces of the brick with the magnetic-field projectors (14) provides equations for the first column of the admittance matrix. Carrying out the same procedure 11 more times or using appropriate substitutions and transformations, we can find the other 11 columns of the matrix. The resulting Y-matrix has exactly the same form (24) as in the case of TFES with the elements defined by (25) and with different expressions for the functions $f_\alpha(p, q)$, $f_\beta(p, q)$, $f_\gamma(p, q)$, and $f_\delta(\Delta)$

$$f_\alpha(p,q)=\frac{p^2\left[q(k_pk_q-2)+k_pk_q+2\right]+q(k_pk_q+2)+k_pk_q-2}{(p-1)f_{dn}(p,q)}$$
$$f_\beta(p,q)=\frac{2\left[p^2(q-1)-p(q+1)k_pk_q-q+1\right]}{(p-1)f_{dn}(p,q)}$$
$$f_\gamma(p,q)=\frac{k_q(p-1)(1-q)}{f_{dn}(p,q)}$$
$$f_{dn}(p,q)=p\left[q(k_pk_q-4)+k_pk_q+4\right]+q(k_pk_q+4)+k_pk_q-4$$
$$f_\delta(\Delta)=\frac{i}{k\Delta}. \quad (37)$$

Note that the expressions (36) for a, b, and k_a, k_b must be substituted into (25) and (37) together with the following expressions for c and k_c:

$$k_c = ik\Delta z \quad c = e^{ik\Delta z}. \quad (38)$$

The Y-matrix of the TFEN can be transformed into the scattering matrix of the brick obtained by the MAB technique [1], [2]. For illustration, consider a brick with all three dimensions equal ($\Delta x = \Delta y = \Delta z = \Delta$). It can be shown that, in this case, we have

$$\begin{aligned} &\alpha_1=\alpha_2=\alpha_3=\alpha_4=\alpha_5=\alpha_6=\alpha \\ &\beta_1=\beta_2=\beta_3=\beta_4=\beta_5=\beta_6=\beta \\ &\gamma_1=\gamma_2=\gamma_3=\gamma_4=\gamma_5=\gamma_6=\gamma \\ &\delta_1=\delta_2=\delta_3=\delta \\ &\alpha=i\cot(k\Delta/2)\left[\frac{2-(k^2\Delta^2+2)\cos(k\Delta)}{f_{dn}}\right] \\ &\beta=i\cot(k\Delta/2)\left[\frac{2\cos(k\Delta)+k^2\Delta^2-2}{f_{dn}}\right] \\ &\gamma=ik\Delta\left[\frac{\cos(k\Delta)-1}{f_{dn}}\right] \\ &f_{dn}=\left(k^2\Delta^2+4\right)\cos(k\Delta)+k^2\Delta^2-4 \\ &\delta=\frac{i}{k\Delta}. \end{aligned} \quad (39)$$

Introducing normalization (29) and new wave variables (30), we can formally define a scattering matrix (31) and express it through the Y-matrix as (32). Substitution of the Y-matrix (24) with the elements defined by (32)–(39) gives the scattering matrix of the cube in (33) with elements defined as

$$\begin{aligned} \varphi &= i\frac{k\Delta I^2}{2(T-I^2)} \\ \chi &= \frac{1-I^2}{T-I^2} \\ I &= \frac{2}{k\Delta}\sin(k\Delta/2) \\ T &= e^{ik\Delta}. \end{aligned} \quad (40)$$

$$S = \begin{bmatrix} 0 & 0 & \chi & 0 & \varphi & 0 & \varphi & 0 & \varphi & 0 & -\varphi & 0 \\ 0 & 0 & 0 & \chi & 0 & \varphi & 0 & -\varphi & 0 & \varphi & 0 & \varphi \\ \chi & 0 & 0 & 0 & \varphi & 0 & \varphi & 0 & -\varphi & 0 & \varphi & 0 \\ 0 & \chi & 0 & 0 & 0 & -\varphi & 0 & \varphi & 0 & \varphi & 0 & \varphi \\ \varphi & 0 & \varphi & 0 & 0 & 0 & \chi & 0 & 0 & \varphi & 0 & -\varphi \\ 0 & \varphi & 0 & -\varphi & 0 & 0 & 0 & \chi & \varphi & 0 & \varphi & 0 \\ \varphi & 0 & \varphi & 0 & \chi & 0 & 0 & 0 & 0 & -\varphi & 0 & \varphi \\ 0 & -\varphi & 0 & \varphi & 0 & \chi & 0 & 0 & \varphi & 0 & \varphi & 0 \\ \varphi & 0 & -\varphi & 0 & 0 & \varphi & 0 & \varphi & 0 & 0 & \chi & 0 \\ 0 & \varphi & 0 & \varphi & \varphi & 0 & -\varphi & 0 & 0 & 0 & 0 & \chi \\ -\varphi & 0 & \varphi & 0 & 0 & \varphi & 0 & \varphi & \chi & 0 & 0 & 0 \\ 0 & \varphi & 0 & \varphi & -\varphi & 0 & \varphi & 0 & 0 & \chi & 0 & 0 \end{bmatrix} \quad (33)$$

Taking into account the difference in the numeration and orientation of the basis functions defined here (11) and in the method of MAB [1], [2], we can conclude that (33) is exactly the same as the one obtained in [1] and [2].

VIII. Assembling Procedure and Boundary Conditions

A global admittance matrix assembling procedure can be defined simultaneously for the TFES and TFEN. Both elements have the same admittance matrices of a brick (24) with different expressions for the elements of the matrices. To define a generalized assembling procedure, we need to define projections of the conduction current density $\vec{j}_{lm}$ on the grid. This can be done in the same way, as the field components are projected on the brick faces. Let us define basis functions for the current density as

$$\begin{aligned}
\begin{pmatrix}\overline{j}_{12(1)}\\ \overline{j}_{12(2)}\end{pmatrix} &= \begin{pmatrix}\overline{z}_0\\ \overline{y}_0\end{pmatrix}, \qquad (x, y, z) \in F_1, F_2\\
\begin{pmatrix}\overline{j}_{34(1)}\\ \overline{j}_{34(2)}\end{pmatrix} &= \begin{pmatrix}\overline{z}_0\\ \overline{x}_0\end{pmatrix}, \qquad (x, y, z) \in F_3, F_4\\
\begin{pmatrix}\overline{j}_{56(1)}\\ \overline{j}_{56(2)}\end{pmatrix} &= \begin{pmatrix}\overline{x}_0\\ \overline{y}_0\end{pmatrix}, \qquad (x, y, z) \in F_5, F_6. \qquad (41)
\end{aligned}$$

Each face of the brick has two orthogonal unit basis vectors. The subscripts in (41) designate that the basis functions will be shared by two faces of two bricks to be united in the assembling procedure. An arbitrary conduction current density on the brick faces can be represented as

$$\vec{J}_{lm} = \sum_{n=1,\,2} I_{lm(n)} \cdot \vec{j}_{lm(n)}, \qquad (x, y, z) \in F_{l,m};$$
$$l = 1; \quad m = 2; \quad l = 3; \quad m = 4; \quad l = 5; \quad m = 6. \qquad (42)$$

A projection of the conduction current on the basis functions can be defined either with a point-matching operator similar to (13) for TFES or with a Galerkin-type projector similar to (14) for TFEN.

To proceed with the generalized assembling procedure, it is convenient to rewrite the system (17) in a block-matrix form, taking into account the structure of the Y-matrix (24)

$$\begin{bmatrix} Y_{11} & Y_{21} & Y_{13} & Y_{23} & Y_{15} & Y_{25}\\ Y_{21} & Y_{11} & Y_{23} & Y_{13} & Y_{25} & Y_{15}\\ Y_{31} & Y_{41} & Y_{33} & Y_{43} & Y_{35} & Y_{45}\\ Y_{41} & Y_{31} & Y_{43} & Y_{33} & Y_{45} & Y_{35}\\ Y_{51} & Y_{61} & Y_{53} & Y_{63} & Y_{55} & Y_{65}\\ Y_{61} & Y_{51} & Y_{63} & Y_{53} & Y_{65} & Y_{55} \end{bmatrix} \cdot \begin{bmatrix} \overline{v}_1\\ \overline{v}_2\\ \overline{v}_3\\ \overline{v}_4\\ \overline{v}_5\\ \overline{v}_6 \end{bmatrix} = \begin{bmatrix} \overline{i}_1\\ \overline{i}_2\\ \overline{i}_3\\ \overline{i}_4\\ \overline{i}_5\\ \overline{i}_6 \end{bmatrix} \qquad (43)$$

where blocks Y_{lm} are 2×2 matrices with elements that can be established by a simple comparison of (24) and (43). Vectors $\overline{v}_m$ and $\overline{i}_l$ are defined by (18).

Let us assume that we need to join brick (A) and brick (B), as is shown in Fig. 3. Faces F_1^A of the brick (A) and F_2^B of the brick (B) coincide. The bricks can be filled with different materials. Joining the bricks, we need to provide a continuity condition for the tangential electric field and continuity or jump conditions for the tangential components of the magnetic field (4). For both bricks, we have necessary projections of the tangential component of the fields (12) defined at the faces F_1^A and F_2^B. They are $\overline{v}_1^A$ and $\overline{i}_1^A$ for the brick (A) and $\overline{v}_2^B$ and $\overline{i}_2^B$ for the brick (B). Vector notations (18) for the face projections are used here. Generalized boundary conditions (4) can be rewritten for the brick boundary as

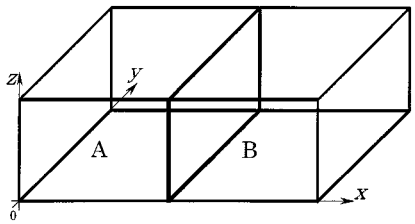

Fig. 3. Joining two bricks.

$$\begin{aligned}
\overline{i}_2^B + \overline{i}_1^A &= \overline{I}_{12}^{AB}\\
\overline{v}_2^B - \overline{v}_1^A &= 0 \qquad (44)
\end{aligned}$$

where $\overline{I}_{12}^{AB}$ is a vector with conduction current components (42) projected on the common boundary between bricks (A) and (B). It is defined in the same way as the vectors $\overline{i}_l$ (18). In general, vectors $\overline{I}$ have zero components where there are no conduction currents. Boundary conditions (44) provide a simple procedure, uniting the Y-matrix descriptors (43) of two bricks, shown in (45), at the bottom of the following page, where $\overline{v}_{12}^{AB} = \overline{v}_1^A = \overline{v}_2^B$ denotes the projections of the electric field on the common boundary (44). The procedure (45) is transparent and recursively applicable to construct a sparse global Y-matrix for the whole grid. Special care must be taken if a face of a brick is interfacing with two or more bricks. This is an important element of the adaptive Cartesian grids [15]. It can be shown that a corresponding numerical procedure can be expressed as simple manipulations with rows and columns of the Y-matrices to be united.

Different boundary conditions can be expressed through an appropriate definition of $\overline{v}$ and $\overline{i}$ values in (45). Ideal metal- or electric-wall boundary conditions are imposed by setting $\overline{v}_l^K = 0$ for all faces F_l^K of elements (K) approximating the metal. This leads to corresponding elimination of rows and columns in the system (45) if the conduction currents are not to be calculated. The same is valid for infinitesimally thin metal layers. For the magnetic wall, we need to set $\overline{i}_l^K = 0$ for all faces F_l^K of elements (K) approximating the boundary. This gives zeroes at the right-hand side of (45), which can, for example, be eliminated using the Gauss's procedure. A hybrid mixed-type descriptor instead of the admittance descriptor can bring those zeroes to the left-hand side, which provides the possibility of eliminating them at the assembling stage. For objects described by its surface impedance, additional equations relating tangential components of the electric field $\overline{v}_{12}^{AB}$ and conduction current density $\overline{I}_{12}^{AB}$ must be taken into account in the assembling procedure.

IX. Numerical Examples

For our first example, let us examine a single brick element, as shown in Fig. 1, with the electric-wall boundary conditions at all faces, except one. The element dimensions are $\Delta x = \Delta y = \Delta z = 0.1$ m. The wavelength is 1.0 m and the element is filled with free space. Let us excite the cube with the unit projection of the z-component of electric field at the face F_1 and find the interior field distribution. To simulate the electric walls, we set all other projections of the electric field on the surface of the brick as zero. The boundary conditions can be expressed as

$$v_{l(m)} = \delta_{l(m),\,1(1)}, \qquad l = 1, \ldots, 6; \quad m = 1,\, 2. \tag{46}$$

To find the field distribution inside the brick, we need to solve the system (22) for the TFES or the system (35) for the TFEN and substitute the expansion coefficients a_{x1}, b_{x1}, a_{y1}, b_{y1} into (7). By doing that, one can obtain expressions for the field components of the TFES

$$\begin{aligned} E_z &= \left(\sqrt{5}+3\right) \cdot \left[-\cos(2\pi x) + \cos\left(2\pi(y-1/20)\right)\right] \\ H_x &= -i\frac{\left(\sqrt{5}+3\right)}{120\pi} \sin\left(2\pi(y-1/20)\right) \\ H_y &= -i\frac{\left(\sqrt{5}+3\right)}{120\pi} \sin(2\pi x). \end{aligned} \tag{47}$$

Thus, we have one component of the electric field E_z and two components of the magnetic field H_x and H_y. They are varying along the x- and y-axes and are constant along the z-direction. The other components are zero. Note that this is the exact solution of the Maxwell's equations (3), but it only approximates the solution of the stated problem. It is obvious from (47) that the projection boundary conditions (46) give zero of E_z only along the z-directed lines going through the centers of F_2, F_3, and F_4, which is expected from the point-matching procedure and is illustrated by a contour plot in Fig. 4(a). Fig. 4(b) shows a vector plot of the corresponding distribution of the magnetic field in the xy-plane of the cube. The solution for the cubic TFEN is slightly more complex as follows:

$$\begin{aligned} E_z &= a_{xr}\cos(2\pi x) + a_{yr}\cos(2\pi y) + a_{xi}\sin(2\pi x) \\ &\quad + a_{yi}\sin(2\pi y) \\ H_x &= i\frac{1}{120\pi}\left(-a_{yr}\sin(2\pi y) + a_{yi}\cos(2\pi y)\right) \\ H_y &= i\frac{1}{120\pi}\left(a_{xr}\sin(2\pi x) - a_{xi}\cos(2\pi x)\right) \\ a_{xr} &= \frac{10\sqrt{5}\left(7-3\sqrt{5}\right)}{f_{dnx}} \\ a_{xi} &= \frac{\pi^2\sqrt{200-40\sqrt{5}} - 10\sqrt{6250-2750\sqrt{5}}}{5f_{dnx}} \\ f_{dnx} &= \pi^2\left(\sqrt{5}-1\right) - 20\sqrt{5}\left(7-3\sqrt{5}\right) \\ a_{yr} &= \frac{-2\pi\sqrt{25/4-5\sqrt{5}/2}}{f_{dny}} \\ a_{yi} &= \frac{\pi\sqrt{5}\left(2-\sqrt{5}\right)}{f_{dny}}, \\ f_{dny} &= \pi^2 + 20\sqrt{5}\left(2-\sqrt{5}\right). \end{aligned} \tag{48}$$

The TFEN solution has the same components E_z, H_x, and H_y varying along the x- and y-axes and constant along the z-direction. The other components are also zero. This is again the exact solution of the Maxwell's equations (3) and it approximates the solution of the stated problem. It is different from the TFES. The projection conditions (46) provide zeros of the integral average values of E_z, defined as (14) on F_2, F_3, and F_4. The field distribution (48) is shown as a contour plot in Fig. 5(a). Fig. 5(b) shows a vector plot of the corresponding distribution of the magnetic field in the xy-plane.

As a second example, let us consider a short-circuited segment of a parallel-plate waveguide excited by the plane wave with the electric field along the z-axis [19]. The example is a simple validation experiment for a noncubic element. The line segment looks like a brick shown in Fig. 1. It is oriented along

$$\begin{bmatrix} Y_{11}^A + Y_{11}^B & Y_{21}^A & Y_{13}^A & Y_{23}^A & Y_{15}^A & Y_{25}^A & Y_{21}^B & Y_{23}^B & Y_{13}^B & Y_{25}^B & Y_{15}^B \\ Y_{21}^A & Y_{11}^A & Y_{23}^A & Y_{13}^A & Y_{25}^A & Y_{15}^A & 0 & 0 & 0 & 0 & 0 \\ Y_{31}^A & Y_{41}^A & Y_{33}^A & Y_{43}^A & Y_{35}^A & Y_{45}^A & 0 & 0 & 0 & 0 & 0 \\ Y_{41}^A & Y_{31}^A & Y_{43}^A & Y_{33}^A & Y_{45}^A & Y_{35}^A & 0 & 0 & 0 & 0 & 0 \\ Y_{51}^A & Y_{61}^A & Y_{53}^A & Y_{63}^A & Y_{55}^A & Y_{65}^A & 0 & 0 & 0 & 0 & 0 \\ Y_{61}^A & Y_{51}^A & Y_{63}^A & Y_{53}^A & Y_{65}^A & Y_{55}^A & 0 & 0 & 0 & 0 & 0 \\ Y_{21}^B & 0 & 0 & 0 & 0 & 0 & Y_{11}^B & Y_{13}^B & Y_{23}^B & Y_{15}^B & Y_{25}^B \\ Y_{41}^B & 0 & 0 & 0 & 0 & 0 & Y_{31}^B & Y_{33}^B & Y_{43}^B & Y_{35}^B & Y_{45}^B \\ Y_{31}^B & 0 & 0 & 0 & 0 & 0 & Y_{41}^B & Y_{43}^B & Y_{33}^B & Y_{45}^B & Y_{35}^B \\ Y_{61}^B & 0 & 0 & 0 & 0 & 0 & Y_{51}^B & Y_{53}^B & Y_{63}^B & Y_{55}^B & Y_{65}^B \\ Y_{51}^B & 0 & 0 & 0 & 0 & 0 & Y_{61}^B & Y_{63}^B & Y_{53}^B & Y_{65}^B & Y_{55}^B \end{bmatrix} \cdot \begin{bmatrix} \overline{v}_{12}^{AB} \\ \overline{v}_2^A \\ \overline{v}_3^A \\ \overline{v}_4^A \\ \overline{v}_5^A \\ \overline{v}_6^A \\ \overline{v}_1^B \\ \overline{v}_3^B \\ \overline{v}_4^B \\ \overline{v}_5^B \\ \overline{v}_6^B \end{bmatrix} = \begin{bmatrix} \overline{I}_{12}^{AB} \\ \overline{i}_2^A \\ \overline{i}_3^A \\ \overline{i}_4^A \\ \overline{i}_5^A \\ \overline{i}_6^A \\ \overline{i}_1^B \\ \overline{i}_3^B \\ \overline{i}_4^B \\ \overline{i}_5^B \\ \overline{i}_6^B \end{bmatrix} \tag{45}$$

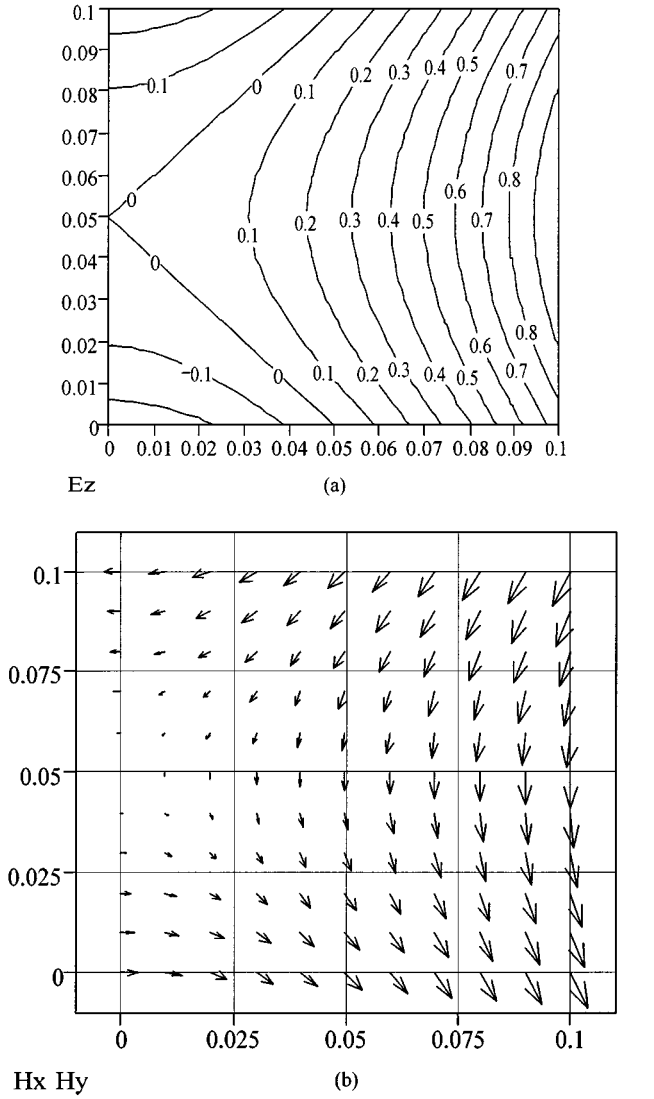

Fig. 4. (a) Contour plot of the z-component of the electric field in the xy-plane of the cubic TFES. (b) Vector plot of the x and y components of the magnetic field in the xy-plane of the cubic TFES.

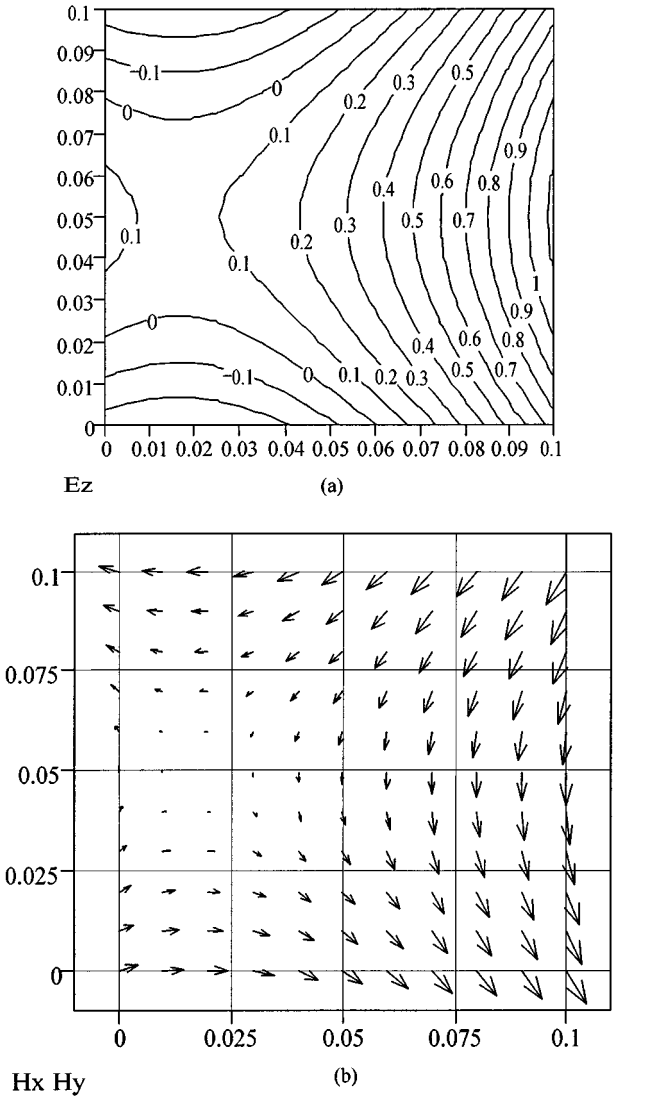

Fig. 5. (a) Contour plot of the z-component of the electric field in the xy-plane of the cubic TFEN. (b) Vector plot of the x and y components of the magnetic field in the xy-plane of the cubic TFEN.

the x-axis, 1.0-m long, and has a square cross section of 0.1 m $\times$ 0.1 m in the zy-plane. Surfaces of the segment parallel to the xy-plane and surface $x = 0$ are electric walls. Surfaces parallel to the xz-plane are magnetic walls. Surface $x = 1.0$ m is excited by the plane wave with a z-component of the electric field. In contrast to the first example, the problem can be solved exactly with only one brick, with $\Delta x = 1.0$ m and $\Delta y = \Delta z = \Delta = 0.1$ m. Corresponding boundary conditions are

$$\begin{aligned} &v_{1(1)} = 1 \\ &v_{1(2)} = v_{2(1)} = v_{2(2)} = v_{5(1)} = v_{5(2)} = v_{6(1)} = v_{6(2)} = 0 \\ &i_{3(1)} = i_{3(2)} = i_{4(1)} = i_{4(2)} = 0. \end{aligned} \tag{49}$$

Substituting (49) into the system (43), we can find $y_{1(1),\,1(1)}$ and then from (32), the reflection coefficient

$$S_{1(1),\,1(1)} = -\frac{\alpha_1(\alpha_3+\beta_3) - \alpha_3 - \beta_3 - 2\gamma_1\gamma_3}{\alpha_1(\alpha_3+\beta_3) + \alpha_3 + \beta_3 - 2\gamma_1\gamma_3} \tag{50}$$

where α_1, α_3, β_3, γ_1, and γ_3 are defined by (25) and either (26) for TFES or (37) for TFEN. We can, for example, check that both elements give the exact value of the reflection coefficient that is the unit magnitude and $-14 - \pi$ phase for the problem with $k = 7$ rad/m.

To verify the matrix assembling procedure, the problem for $k = 7$ rad/m was also solved numerically for different number of bricks along the coordinate axes. The input impedance for the plane wave at $x = 1.0$ m is calculated using a recursive procedure of an admittance matrix assembling and reduction for one layer of the bricks in the yz-plane at a time [2]. The structure was simulated starting from just one brick and up to 64 $\times$ 16 $\times$ 16 bricks with both TFES and TFEN admittance matrices. The calculated input impedance is $i328.300\,868\ \Omega$. The result was independent of the number of bricks. That gives the value of the reflection coefficient of the plane wave 1.70796327 rad, which corresponds to the exact theoretical value $-14 - \pi$.

As a last example, let us consider a segment of a parallel-plate waveguide excited by the plane wave with the electric field

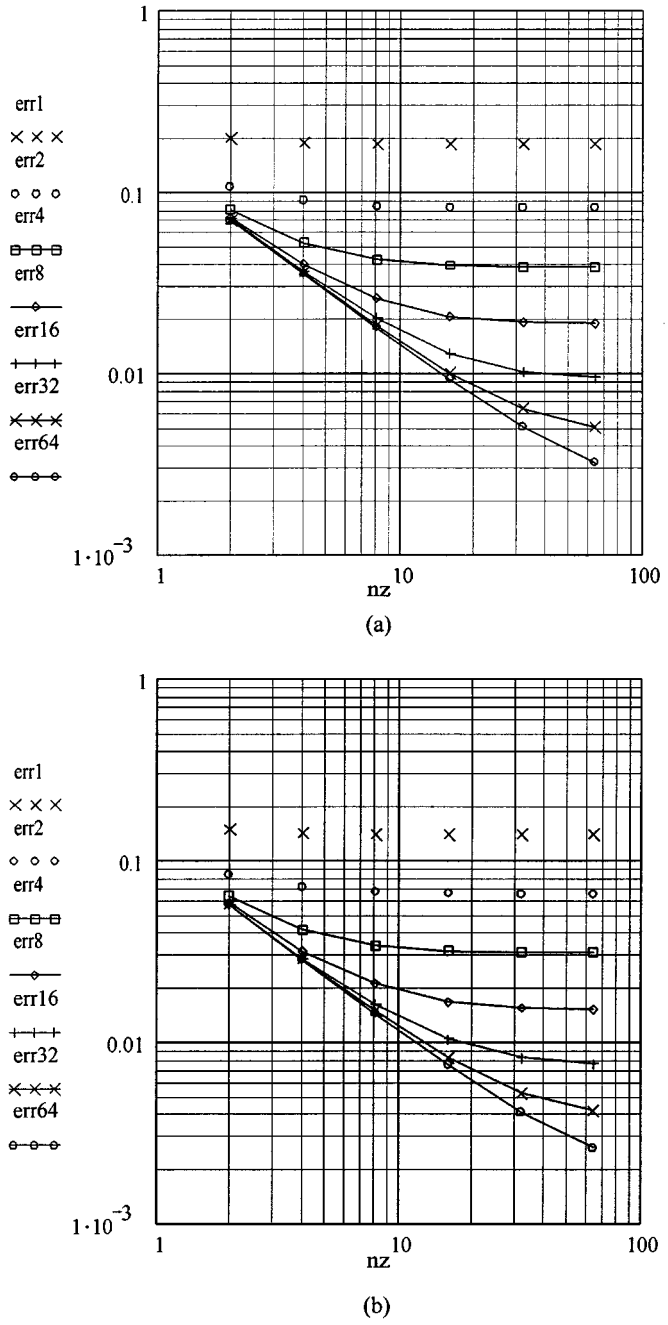

Fig. 6. Parallel-plate waveguide partially blocked by a conductive plate simulated: (a) with TFES bricks and (b) with TFEN bricks. The relative errors $\mathrm{err}N$ for different number of bricks N along the x-axis are plotted versus the number of the bricks along the z-axis nz.

along the z-axis and partially blocked by a conductive plate [19]. The example shows the convergence of the method for a problem with a field singularity. Again, the line segment looks like a brick, as shown in Fig. 1. It is oriented along the x-axis, 1.0-m long, and has a square cross section of 1.0 m $\times$ 1.0 m in the zy-plane. Surfaces of the segment at $z = 0$ and $z =$ 1.0 m are electric walls. Surfaces at $y = 0$ and $y = 1.0$ m are magnetic walls. A surface at $x = 0$ is divided into two areas. It is an electric wall for $z < 1/2$ m and a magnetic wall for $z > 1/2$ m. The problem is simulated for medium with $k = 1$ rad/m. The input impedance of the plane wave was estimated for a different number of bricks and normalized to the input impedance of free space to get the phase of the reflection coefficient. For the TFES, the phase was -2.46546626 rad with 32 elements along the x-axis and 32 elements along the z-axis, and -2.45764825 rad with 64 $\times$ 64 elements. These values were independent of the discretization along the y-axis (problems with one, two, and four elements along the y-axis were simulated). The Richardson's extrapolation on those two grids gives phase value -2.4498302 rad, which is considered to be exact here to estimate calculation errors. The relative calculation errors $\mathrm{err}N$ are plotted in Fig. 6(a) as functions of the number of bricks along the z-axis (nz). N in $\mathrm{err}N$ designates the number of bricks along the x-axis. Simulation of the problem with TFENs gives phase -2.46256247 rad for 32 $\times$ 32 elements and -2.45620889 rad for 64 $\times$ 64 elements. Again, it is supposed that the Richardson's extrapolation provides a more accurate value of the phase that is -2.4498553 rad. It coincides with the TFES result up to the fourth digit after the decimal point. As in the case of TFES, the relative calculation errors with respect to the value considered as exact are shown in Fig. 6(b). Both TFES and TFEN show good convergence and consistent results. Note that TFEN provides slightly better accuracy for the problem. Magnitudes of the reflection coefficients were units in all experiments.

X. Conclusion

It was shown that the method of MAB can be reformulated and generalized as the TFE method. It is suggested to use a plane-wave solution of Maxwell's equations as the intra-element basis functions. The element descriptor construction procedure based on the integration over the element boundaries only is proposed. Two different descriptors of a brick-shaped element in the form of admittance matrices have been constructed and investigated as examples. It was shown that the expansion of the brick interior field into 12 plane waves combined with a projection on the brick surface with the point-matching procedure can be considered as a derivation procedure for the frequency-domain TLM condensed node. The same intra-element field expansion combined with the Galerkin-type projectors on the surface lead to the admittance matrix, which was then converted into the scattering matrix descriptor of MAB.

Elements of different shapes with polygonal and curvilinear boundaries can be constructed following the procedure. The intra-element basis functions can be optimized (varying the type and number of the plane waves) to increase the element order and to take into account some peculiarities of a problem. It can be done independently from the surrounding elements because the inter-element continuity is not required at the element building stage. It was also shown that the admittance form of the element descriptors provides a simple global matrix assembling procedure.

References

[1] V. V. Nikol'skii and T. I. Lavrova, "The method of minimum autonomous blocks and its application to waveguide diffraction problems," *Radio Eng. Electron. Phys.*, vol. 23, no. 2, pp. 1–10, 1978.

[2] V. V. Nikol'skii and T. I. Nikol'skaia, *Decompositional Approach to Electromagnetic Problems* (in Russian). Moscow, Russia: Nauka, 1983.

[3] G. Kron, "Equivalent circuit of the field equations of Maxwell," *Proc. IRE*, vol. 32, pp. 289–299, May 1944.

[4] B. V. Sestroretzkii, "Balanced *RLC*- and $R\tau$-circuits of elementary volumes of space" (in Russian), *Vopr. Radioelektron.*, ser. OVR, no. 5, pp. 56–85, 1983.
[5] P. B. Johns, "A symmetrical condensed node for the TLM method," *IEEE Trans. Microwave Theory Tech.*, vol. MTT-35, pp. 370–377, Apr. 1987.
[6] H. Jin and R. Vahldieck, "The frequency-domain transmission line matrix method—A new concept," *IEEE Trans. Microwave Theory Tech.*, vol. 40, pp. 2207–2218, Dec. 1992.
[7] Z. Chen, M. M. Ney, and W. J. R. Hoefer, "A new finite-difference time-domain formulation and its equivalence with the TLM symmetrical condensed node," *IEEE Trans. Microwave Theory Tech.*, vol. 39, pp. 2160–2169, Dec. 1991.
[8] H. Jin, R. Vahldieck, and J. Huang, "Direct derivation of the TLM symmetrical condensed node from Maxwell's equations using centered differencing and averaging," in *IEEE MTT-S Int. Microwave Symp. Dig.*, 1994, pp. 23–26.
[9] M. Krumpholz and P. Russer, "A field theoretical derivation of TLM," *IEEE Trans. Microwave Theory Tech.*, vol. 42, pp. 1660–1668, Sept. 1994.
[10] V. M. Seredov, "Reduction of a system of partial differential equations to local approximation form" (in Russian), *Vopr. Radioelektron.*, ser. OVR, no. 12, pp. 50–60, 1985.
[11] O. C. Zienkiewicz and R. L. Taylor, *The Finite Element Method: Basic Formulation and Linear Problems*. New York: McGraw-Hill, 1994.
[12] V. V. Nikol'skii and T. I. Lavrova, "Solution of characteristic mode problems by the method of minimum autonomous blocks," *Radio Eng. Electron. Phys.*, vol. 24, no. 8, pp. 26–33, 1979.
[13] Y. O. Shlepnev, B. V. Sestroretzkii, and V. Y. Kustov, "A new approach to modeling arbitrary transmission lines," *J. Commun. Technol. Electron.*, vol. 42, no. 1, pp. 13–16, 1997.
[14] Y. O. Shlepnev, "A new generalized de-embedding method for numerical electromagnetic analysis," in *Proc. 14th Annu. Rev. Progress Appl. Comput. Electromagn.*, Mar. 1998, pp. 664–671.
[15] M. J. Aftosmis, M. J. Berger, and J. M. Melton, "Adaptive Cartesian mesh generation," in *Handbook of Grid Generation*, J. F. Thompson, B. K. Soni, and N. P. Weatherill, Eds. Boca Raton, FL: CRC Press, 1998, pp. 22/1–22/26.
[16] A. F. Peterson, S. L. Ray, and R. Mittra, *Computational Methods for Electromagnetics*. Piscataway, NJ: IEEE Press, 1998.
[17] B. V. Sestroretzkii and V. Y. Kustov, "Electromagnetic simulation of multi-layer integrated structures on the base of *RLC*-networks and the method of informational multiport" (in Russian), *Vopr. Radioelektron.*, ser. OVR, no. 1, pp. 3–23, 1987.
[18] J. Huang, R. Vahldieck, and H. Jin, "A new frequency-domain TLM algorithm using a decoupled symmetrical condensed node," in *IEEE MTT-S Int. Microwave Symp. Dig.*, 1994, pp. 1535–1538.
[19] J. P. Webb, "Hierarchal vector basis functions of arbitrary order for triangular and tetrahedral finite elements," *IEEE Trans. Microwave Theory Tech.*, vol. 47, pp. 1244–1253, Aug. 1999.

Yuriy Olegovich Shlepnev (M'99) was born in Mogzon, Russia, in 1963. He graduated from the School of Physics and Mathematics of M. Lavrent'ev, Novosibirsk, Russia, in 1979, and received the Engineer degree (M.S.) in radio engineering from the Novosibirsk State Technical University, Novosibirsk, Russia, in 1983, and the Candidate of Technical Science degree (Ph.D.) in electrical engineering from the Novosibirsk Electrical Engineering Institute of Communication, Novosibirsk, Russia, in 1990. His doctoral dissertation concerned the development of a complete set of algorithms for 3-D electromagnetic simulation of elements of integrated circuits (ICs) on the base of the method of lines and multimode decomposition technique.

From 1983 to 1991, he was with the Department of Transmitters and Receivers, Scientific Research Laboratory, Novosibirsk State Technical University. In 1992, he joined the TAMIC Software Group, Moscow, Russia, where he was responsible for the development of electromagnetic software for simulation of microwave ICs. From 1997 to 2000, he was Principal Developer of the planar 3-D electromagnetic simulation software for the Eagleware Corporation, Atlanta, GA. He is currently a Principal Engineer with Innoveda Inc., Camarillo, CA, where he is involved with electromagnetic software for simulation of high-frequency and high-speed digital circuits.